Nano-indentation mapping of fretting-induced surface layers

T. Liskiewicz[1], K. Kubiak[2], T. Comyn[3]

1. School of Mechanical Engineering, University of Leeds, Leeds, UK

2. School of Computing & Engineering, University of Huddersfield, Huddersfield, UK

3. Ionix Advanced Technologies, Huddersfield, UK

Abstract

Tribologically modified surface layer results from the energy dissipated in the frictional contact area. This layer usually has a different elastic modulus and hardness from the substrate, and its structure corresponds to the intermediate stage between a material of the first-body and debris of the third-body. Even though, the existence of the tribologically transformed structure in the fretting contact has been well proven, the formation and mechanical transformation mechanisms are still not clear. Hence, in this paper, evolution of mechanical properties of four metallic materials (titanium alloy, stainless steel, carbon steel, copper alloy) induced by fretting was investigated using nano-indentation mapping of the fretting wear scars. It was shown that the tribologically transformed structure formed very quickly within the initial fretting cycles, and its mechanical properties remained almost constant during the entire test duration for tested materials. However, it was observed that all materials responded differently to the frictional energy, exhibiting particular rate of change of the H/E ratio before and after the fretting experiment. Modified XRD technique was used to probe the friction induced changes within the small spots of the fretting scars, and revealed distinctive structural modifications within the transformed layers. The approach proposed in this study can be used to inform the predictive

wear models, by providing information about the evolution of the mechanical properties of the tribo-system with time.

1. Introduction

During the wear process, the crystallographic structure, physical and chemical properties of the surface layer within the tribological contact area are subjected to dynamic changes. It was proposed that degradation of the surface layer is rather associated with the quantity of debris ejected outside the contact area, than with the total wear volume [1]. Debris remaining in the contact participate in the process of load transmission and protect indirectly the first-bodies against degradation. In this case, the following statement can be quoted: 'a good anti-wear material combination is one that sacrifices its surface to save its volume' [2]. The third-body can be introduced to the interface voluntary (e.g. solid lubricant, grease, oil), or can result from the wear process of the first-bodies, leading to debris screen being maintained within the contact area.

By a successive observation of the friction interface [3], five different sites (S_i) and four interaction modes (M_j) have been defined in the contact area (Figure 1). The five sites are two rubbing solids, a "bulk" third-body and two screens separating the first-bodies from the bulk third-body; while the four interaction modes are the elastic, rupture, shear and rolling modes. The accommodation mechanism was then defined as the S_iM_j couple, and 20 different combinations can be identified.

Fretting wear is a specific surface damage process, where the reciprocating sliding motion with a relatively small amplitude is responsible for the debris formation and loss of material as a result of the interfacial shear work. Prediction of fretting wear rates and its mechanism is challenging, due to a number of specific factors including [4-6]: (i) high-frequency

modification of the interface and contact geometry during the wear process, (ii) occurrence of the third-body within the contact area, (iii) flow of debris, and (iv) mechanisms of material transport between mated bodies. Nevertheless, it was observed [7], that third-body screens S2 and S4 are also activated during fretting wear process.

Further studies of the third-body layers shown that metallic materials subjected to alternating sliding, tend to generate a specific transformed layer on the top surface [8,9]. This layer, called Tribologically Transformed Structure (TTS), has a particular nanocrystalline structure, corresponding to the chemical composition of the primary material.

Tribologically Transformed Structure results from plastics deformations induced by a relative motion of solid bodies under load, and usually has a different elastic modulus and hardness from the original metallic structure. The transformed layer corresponds to the intermediate stage between a material of the first-body and debris of the third-body. E. Sauger studied various titanium tribo-systems and the following two-stage wear mechanism was proposed [10]: (i) accumulation of plastic deformation (without wear and TTS formation), and (ii) rapid formation of TTS leading to generation of wear debris. It was shown by the same author that the thickness of the TTS layer remains constant afterwards, while total wear volume increases following the TTS to wear debris transformation process.

Even though, the existence of the TTS layer in the fretting contact has been well proven, the formation and transformation mechanisms are still not clear. Further understanding of this process will have a significant consequences for the reliability of wear models, and overall prediction of the tribological performance of components under fretting regime. However, the TTS formation process, and mechanical properties of the transformed structure will be unique for different materials. Hence, in this paper, evolution of mechanical properties of four metallic materials induced by fretting is investigated using nano-indentation mapping of the

fretting wear scars. The process is related to the dynamics of the TTS formation and successive surface damage.

2. Methods

2.1. Materials

Four commonly used engineering materials were selected for this study: titanium alloy (Ti6Al4V), stainless steel (316L), carbon steel (C50) and copper alloy (UNS C17000). Test coupons were machined to 10x10x20 mm samples and tested against 225 mm diameter alumina ball. The mechanical properties of materials used in this study are presented in Table 1.

2.2. Fretting experiments

A dedicated, electro-dynamic shaker powered fretting setup built in School of Mechanical Engineering at the University of Leeds was used in this study [11]. All experiments were carried out in dry conditions, at 5 Hz frequency, under 20-80 N normal load, in ambient laboratory conditions at the temperature of 22°C and relative humidity between 40% and 55%. The experiments were performed under gross-slip fretting conditions with ±100μm displacement amplitude. After fretting experiments, the wear volume was characterised using optical profiler (NPFLEX 3D, Bruker).

2.3. Nano-indentation

Hardness and elastic modulus maps were produced using pendulum-based nano-indention platform (NanoTest, Micro Materials Limited) [12]. For each map, 10x10 indentation matrix was generated. The spacing between individual indents was designed in such a way, so that the whole fretting wear scar was within the measurement area. The peak load used in the nano-

indentation tests was 50mN. The Oliver and Pharr method was used to analyse the nano-indentation data [13]. The graphical representation of hardness and elastic modulus was then generated by the NanoTest platform software.

2.4. XRD analysis

XRD technique was used in this study to compare the crystal structure of the original material with worn surfaces. The main motivation to carry out these experiments was to investigate the modification to surface structure induced by wear. The equipment used was P'Analytical X'Pert MPD, with Cu $K\alpha_1/\alpha_2$ radiation. In order to investigate a limited area of the sample surface with the wear scar, the tube was set up in point focus and cup collimators were used, providing an approximate beam size of 2x2 mm at $2\theta = 40°$. Note this changes with incident angle, and is far smaller for high 2θ, ca. 1x2 mm. This method resulted in slightly worse statistics than in conventional line focus mode as the flux was far lower, requiring longer scan times. A fluorescent disk was used to find the X-ray beam on the sample surface – a fine red laser spot was used to align the sample to irradiated zone. Scans were performed in both, the worn region, and in perimeter away from damage.

3. Results

3.1. Wear behaviour

Figure 2 shows fretting wear volume of four tested materials as a function of cumulated dissipated energy, rather than the number of fretting cycles. This approach allows to quantify the normal load, displacement amplitude, fretting test duration, and evolution of the coefficient of friction by a single function and correlate all those parameters to the extent of wear [14-16]. It is also possible to determine the energy wear coefficient (tangent of the line function), and

compare fretting wear resistance of tested materials. The titanium alloy showed low wear resistance comparing to the other three materials under applied fretting conditions.

3.2. Hardness and Elastic Modulus maps

A selection of hardness and elastic modulus nano-indentation maps is presented here. The results are split into three sections illustrating the impact of (i) four materials tested, (ii) test duration, and (iii) applied normal load. The 10x10 nano-indentation matrix was arranged in such a way, so that the entire wear scar with the surrounding virgin surface was characterised. It required adjustment of the matrix size between the samples, as the fretting wear scar size varied between the tests depending on the test duration and loads applied.

3.2.1. Impact of materials

A clear drop of both, hardness and elastic modulus was observed for the titanium alloy within the fretting wear scar when compared with the surrounding, unmodified by friction surface (Figure 3). A very different behaviour was shown by the copper sample, where significant increase of hardness was observed, accompanied by a moderate drop of the elastic modulus. The stainless steel and carbon steel samples showed an intermediate behaviour with varied hardness, and a drop of elastic modulus – more apparent for the stainless steel sample.

3.2.2. Impact of test duration

Figure 4 shows hardness and elastic modulus of the titanium alloy sample after 10000 cycles fretting test. When compared with Figure 3a-b (2000 cycles fretting test on titanium alloy), impact of the test duration can be observed. The elastic modulus map morphology is very

similar in both cases, however the hardness map shows more distinct crater-like shape. The wear scar areas became slightly larger, as illustrated by longer Y and Z stage scanning lengths: 2100µm (Fig. 4) vs. 1600µm (Fig. 3).

3.2.3. Impact of applied normal load

Figure 5 shows hardness and elastic modulus of the titanium alloy sample after fretting test under 80N normal load. When compared with Figure 3a-b (20N normal load fretting test on titanium alloy), impact of the loading condition can be observed. The absolute hardness and modulus values are very similar in both cases, however the crater-like shapes representing the fretting wear scars are much more distinct for the test under higher load. The wear scar areas became also much larger, as illustrated by longer Y and Z stage scanning lengths: 3100µm (Fig. 5) vs. 1600µm (Fig. 3).

3.3. XRD analysis

All four materials were studied using XRD to investigate the modification to surface structures induced by wear.

No change in peaks position, breadth, shape or relative intensity was observed for Ti6Al4V alloy between the wear region and virgin sample surface. However, the intensity of peaks was reduced uniformly (Figure 6). Relatively large increase in background signal was observed at all angles, and particularly centred on $2\theta = 40^{o}$, which may be interpreted by amorphous layer formed at surface, obscuring the crystalline sub-layer structure. The penetration depth normal to the sample surface vs. diffraction angle can be calculated using mass absorption coefficients, with the knowledge of angle, material and density [17]. By doing so, it has been revealed that

at 40°, near strong Bragg peaks, 99% of diffraction occurs at a depth <8.9 μm from the surface (value based on 99% absorbed and 1% transmitted signal).

A slight increase in peak intensity and background signal was observed at low angles for carbon steel sample, when comparing the worn region to the virgin sample surface. Additionally, an increase in Bragg peak breadth was observed, which was attributed to an increase in micro-strain. The micro-strain in the surface layer was calculated from the maximum breadth of peaks at different angles (lowest penetration depth at low angles). Increased strain was observed at the low penetration depths of the worn sample, comparing to the higher penetration depths, indicating micro-strain induced by friction (Table 2), resulting in plastic deformation.

No particular change in the background signal was observed for 316L steel samples when comparing the wear region to the virgin sample surface, however non-uniform change in the peaks height was observed (Figure 8). To investigate it further, the samples were rotated, such that the impinging X-rays were parallel or perpendicular to the wear scars. This resulted in large change in peak position, and intensity, suggesting a presence of a layer with residual stress and preferred crystallographic orientation. Additionally, a peak at 44.7° was observed in some samples, which might result from austenitic/martensitic phase transformation.

When using a small X-ray spot size, away from the wear regions on copper, only tiny Bragg peaks were recorded (Figure 9). In comparison, very distinct but limited Bragg peaks could be seen in the wear region: (111) at ca. 43° and (222) at ca. 94°. This suggests, that highly modified, amorphous (polished) surface, was present in the top layer of copper sample before the tribological test, which was removed by wear resulting in the structure with highly preferred crystallographic orientation.

4. Discussion

Progressive wear volume measurement is a typical way of characterising the material durability under given tribological conditions. Figure 2 shows the wear volume as a function of cumulated dissipated energy for four tested materials in this study. The titanium alloy showed the poorest performance comparing to the other three materials, however, the main objective of this study was to explore the link between the progressive wear process and development of the third-body screen within the fretting contact area. As highlighted in the introduction section, metallic materials subjected to alternating sliding tend to generate tribologically transformed structure, with a particular structure corresponding to the chemical composition of the primary material. Under successive fretting cycles TTS is fragmented and the wear scar becomes saturated with debris. Wear debris is then subjected to the progressive oxidation process and, as a result, sliding surfaces are separated by a fully oxidized particles film [18]. Hence, the aim of this study was to investigate tribological implications of friction-induced surface modification of metallic materials induced by fretting by characterising the mechanical properties of the TTS structures using nano-indentation mapping concept.

Very different mechanical response to the tribological load can be seen in Figure 3 for the four tested materials. The TTS layer was not always characterised by increased hardness due to energy dissipated in the contact area and work hardening. The surface of copper was clearly work hardened, however the titanium alloy was softened. Moreover, the extent of change of the elastic modulus varied between the materials, with the stainless steel showing the largest drop, and copper the smallest.

The TTS formation process involves complex competition between surface strain hardening, and wear debris generation and oxidation. The former leads to harder surface, while the latter leads to wear particles generation. Fragmented wear particles will result in a porous structure, which may affect the hardness and elastic modulus nano-indentation measurements. Ti-6Al-4V alloy and steels are found to have moderate strain hardening behaviour, comparing to

copper, which can be easily strengthened via work hardening [19, 20]. It is also worth mentioning the link between stacking-fault energy (SFE) and strain hardening, as metals and alloys with wider stacking faults (low SFE) like stainless steels, strain harden more rapidly [21, 22].

Individual peaks diverging from the average neighbouring measurement values can be observed within the wear scars in Figure 3. These anomalies relate to the single indents resulting from increased roughness and porous nature of the modified material within the wear scars [23]. In fact, high porosity of the TTS layer may lead to low elastic modulus of the fretted samples due to the size effect of the nano-indentation test. Figures 4 and 5 show that the method can be used to measure the progressive wear with increasing test duration or increased normal load. In both cases, the extent of change of hardness and elastic modulus is becoming more distinctive as compared to the shorter test or test carried out under lower normal load (Figure 3a-b).

Small-scale fretting on Ti alloys and on copper was investigated by T. Hanlon and A. Singh at MIT [24, 25]. The authors performed nano-indentation tests at the base of the sliding tracks to assess local gradients in mechanical properties. Their results on copper indicated that local mechanical response within wear scars, was more strongly influenced by local structure evolution during repeated sliding than by the initial structure. It was also observed that both, friction and damage evolution, were dominated by material strength, when different nanocrystalline materials were compared. The authors concluded, that those strengthening mechanisms, rather than grain refinement, could provide a more economically viable means of improving tribological resistance.

The specific XRD setup used in this study allowed performing structural analysis, by comparing the friction-modified surfaces within the fretting wear scars, with those unchanged by friction. It is evident that more detailed study is required to improve quantitative

correlation of the tribological conditions with the rate and nature of crystallographic changes measured. However, it has been showed that the method is capable of probing the friction induced changes within the small spots of the fretting scars. It was observed that the titanium alloy showed amorphous layer formed at the surface, carbon steel showed an increase in micro-strain (with actual strain value calculated as a function of TTS layer thickness – Table 2), stainless steel showed a presence of a layer with residual stress and preferred crystallographic orientation, and copper sample showed evidence of structure with modified crystallographic morphology.

In summary, it has to be highlighted, that within a few initial fretting cycles, the mechanical properties of the materials are dramatically changed. The hardness and elastic modulus values become very different to the ones in the original material specification. The process can be related to as "in-situ local friction-induced surface modification". Figures 10 and 11 illustrate that fact in a clear graphical way. Figure 10 shows the extent of change of hardness, while Figure 11 shows the extent of change of elastic modulus of the four tested materials. In both cases, value zero on the vertical axis represents the initial hardness and elastic modulus values before the tests. The further away the data points from the initial zero value, the more dramatic change of the mechanical properties resulting from friction induced surface modification took place. It is interesting to observe, that after initial change, the values remain relatively constant. It suggests, that the energy dissipated with the initial fretting cycles, promotes the TTS structure, and as a result, the tribological system is modified very quickly. This supports the observation, that the thickness of the TTS layer remains constant after formation, while total wear volume increases following the continuous process of TTS transformation to wear debris [10].

The observed phenomenon of friction-induced surface modification of metallic materials under fretting, will have implications for predictive wear models and numerical calculations

of tribo-contacts durability. These are typically based on initial mechanical properties of materials measured prior to service, and do not take into account the adjusted values of hardness and elastic modulus. This will also change the H/E and H^3/E^2 parameters [26,27], which are considered to be useful in prediction of tribological performance of materials.

5. Conclusions

The tribological significance of friction-induced surface modification of metallic materials under fretting regime was investigated in this study. The nano-indentation mapping approach was used to measure the hardness and elastic modulus values within the fretting wear scars on titanium alloy (Ti6Al4V), stainless steel (316L), carbon steel (C50) and copper alloy (UNS C17000) samples. The following conclusions can be drawn from this study:

- Nano-indentation mapping proved to be a powerful technique allowing to quantitatively resolve the mechanical properties of Tribologically Transformed Structure within the fretting scars, and compare with the original material.
- It was shown that the Tribologically Transformed Structure formed very quickly within the initial fretting cycles, and its mechanical properties remained almost constant during entire test duration for all four tested materials.
- Materials investigated in this study reacted differently to the energy dissipated with the contact area, exhibiting particular rate of change of hardness and elastic modulus. This resulted in different H/E ratio values for the same material before and after the fretting experiment.
- Modified XRD technique used in this study allowed probing the friction induced changes within the small spots of fretting scars. It revealed distinctive structural changes within the

TTS layers, and allowed calculation of the micro-strain as a function of TTS layer thickness for carbon steel.

- The study quantified the in-situ local friction-induced surface modification process taking place during fretting wear. This approach can be used to inform the predictive wear models, by understanding the evolution of the mechanical properties of the tribosystem.

References

1. Godet M. The third-body approach: a mechanical view of wear. Wear 1984;100:437-52.
2. Berthier Y, Vincent L, Godet M. Fretting fatigue and fretting wear. Tribology International 1989;22:235-42.
3. Berthier Y, Vincent L, Godet M. Velocity accommodation in fretting. Wear 1988;106:25-38.
4. Vingsbo O, Söderberg S. On fretting maps. Wear 1988;126(2):131–47
5. Jin O, Mall S. Effects of slip on fretting behavior: experiments and analyses. Wear 2004;256(7–8):671–84.
6. McColl IR, Ding J, Leen SB. Finite element simulation and experimental validation of fretting wear. Wear 2004;256(11–12):1114–27.
7. Vincent L, Berthier Y, Dubourg MC, Godet M. Mechanisms and materials in fretting. Wear 1992;153:135-48.
8. Blanchard P. Usure induite en petits débattements: TTS d'alliages de titane. Thèse Ecole Centrale de Lyon, No 91-32 (1991).
9. Sauger E, Fouvry S, Ponsonnet L, Kapsa Ph, Martin JM, Vincent L. Tribologically transformed structure in fretting. Wear 2000;245:39-52.
10. Sauger E. Contribution à l'étude de la transformation tribologique superficielle en fretting. Thèse Ecole Centrale de Lyon, No 97-25 (1997).

11. Kubiak KJ, Liskiewicz TW, Mathia TG. Surface morphology in engineering applications:Influence of roughness on sliding and wear in dry fretting. Tribology International 2011;44:1427-32.
12. Beake BD, Liskiewicz TW, Vishnyakov VM, Davies MI. Development of DLC coating architectures for demanding functional surface applications through nano- and micro-mechanical testing. Surface and Coatings Technology 2015;284:334-43.
13. Pharr GM, Oliver WC, Brotzen FR. On the generality of the relationship among contact stiffness, contact area, and elastic-modulus during indentation. Journal of Materials Research 1992;7(3):613-7.
14. Fouvry S, Kapsa Ph, Vincent L. Quantification of fretting damage. Wear 1996;200:186-205.
15. Liskiewicz T, Fouvry S. Development of a friction energy capacity approach to predict the surface coating endurance under complex oscillating sliding conditions. Tribology International 2005;38:69-79.
16. Fouvry S, Liskiewicz T, Paulin C, A global–local wear approach to quantify the contact endurance under reciprocating-fretting sliding conditions. Wear 2007;263:518-31.
17. International Tables for Crystallography, Vol. C, Mathematical, Physical and Chemical Tables, ed.: Wilson, A.J.C, Kluwer, London (1995).
18. Busquet M, Descartes S, Berthier Y. Formation conditions of mechanically modified superficial structures for two steels. Tribology International 2009;42(11–12):1730-43.
19. Estrin Y, Mecking H. A unified phenomenological description of work hardening and creep based on one-parameter models. Acta Metallurgica 1984;32(1):57-70.
20. Gupta RK, Mathew C, Ramkumar P. Strain Hardening in Aerospace Alloys. Frontiers in Aerospace Engineering 2015;4(1):1-13.

21. Peng X, Zhu D, Hu Z, Yi W, Liu H, Wang M. Stacking fault energy and tensile deformation behavior of high-carbon twinning-induced plasticity steels: Effect of Cu addition. Materials & Design 2013;45:518-23.
22. Das A. Revisiting Stacking Fault Energy of Steels. Metallurgical and Materials Transactions A 2016;47(2):748-68.
23. Lemm JD, Warmuth AR, Pearson SR, Shipway PH. The influence of surface hardness on the fretting wear of steel pairs—Its role in debris retention in the contact. Tribology International 2015;81:258-66.
24. Hanlon T, Chokshi AH, Manoharan M, Suresh S. Effects of grain refinement and strength on friction and damage evolution under repeated sliding contact in nanostructured metals. International Journal of Fatigue 2005;27:1159-63.
25. Singh A, Dao M, Lu L, Suresh S. Deformation, structural changes and damage evolution in nanotwinned copper under repeated frictional contact sliding. Acta Materialia 2011;59:7311-24.
26. Leyland A, Matthews A. On the significance of the H/E ratio in wear control: a nanocomposite coating approach to optimised tribological behaviour. Wear 2000;246(1–2):1-11.
27. Liskiewicz TW, Beake BD, Schwarzer N, Davies MI. Short note on improved integration of mechanical testing in predictive wear models. Surface & Coatings Technology 2013;237:212-18.

Table 1. Mechanical properties of tested materials.

Material	Hardness (GPa)	Elastic Modulus (GPa)	Residual depth/ Max depth
Titanium alloy (Ti6Al4V)	4.7 ±0.2	156.4 ±8.8	0.91 ±0.01
Stainless steel (316L)	2.9 ±0.1	221.9 ±6.3	0.96 ±0.01
Carbon steel (C50)	3.4 ±0.4	249.3 ±7.8	0.96 ±0.01
Copper alloy (UNS C17000)	1.3 ±0.1	135.3 ±6.0	0.97 ±0.01

Table 2. Micro-strain calculations in the surface layer of worn carbon steel sample.

Test position	FWHM* / º	FWHM* (Si) / º	Peak pos. / º	Micro-strain / %	Micro-strain change
Virgin	0.287	0.230	44.700	0.182	**+0.078**
Wear scar	0.336	0.230	44.700	0.260	
Virgin	0.460	0.240	65.070	0.268	**+0.055**
Wear scar	0.530	0.240	65.070	0.323	
Virgin	0.510	0.250	82.390	0.222	**+0.016**
Wear scar	0.539	0.250	82.390	0.238	
Virgin	0.513	0.250	98.870	0.167	**-0.009**
Wear scar	0.491	0.250	98.870	0.158	

* FWHM - full width at half maximum

Fig. 1. Frictional energy accommodation mechanisms in the fretting contact (Own diagram after [3]).

Fig. 2. Fretting wear volume of four tested materials as a function of cumulated dissipated energy.

Fig. 3. Hardness and elastic modulus maps for four tested materials; Test conditions: ±100μm displacement amplitude, 5HZ frequency, 20N normal load, 2000 fretting cycles; a-b) titanium alloy (Ti6Al4V), c-d) stainless steel (316L), e-f) carbon steel (C50), and g-h) copper alloy (UNS C17000).

Fig. 4. Hardness and elastic modulus maps for titanium alloy (Ti6Al4V); Test conditions: ±100μm displacement amplitude, 5HZ frequency, 20N normal load, 10000 fretting cycles.

Fig. 5. Hardness and elastic modulus maps for titanium alloy (Ti6Al4V); Test conditions: ±100μm displacement amplitude, 5HZ frequency, 80N normal load, 2000 fretting cycles.

Fig. 6. XRD spectrum for Ti6Al4V; dark line – virgin region of the sample;
light line – worn surface.

Fig. 7. XRD Bragg peaks for carbon steel; dark line – virgin region of the sample;
light line – worn surface.

Fig. 8. XRD Bragg peaks for 316L steel; dark line – virgin region of the sample;
light lines – worn surface, parallel and perpendicular X-ray scans.

Fig. 9. XRD spectrum for copper; top line – virgin region of the sample;
bottom line – worn surface.

Fig. 10. Variation of hardness for four tested materials as a function of cumulated dissipated energy.

Fig. 11. Variation of Elastic Modulus for four tested materials as a function of cumulated dissipated energy.

Figure 1

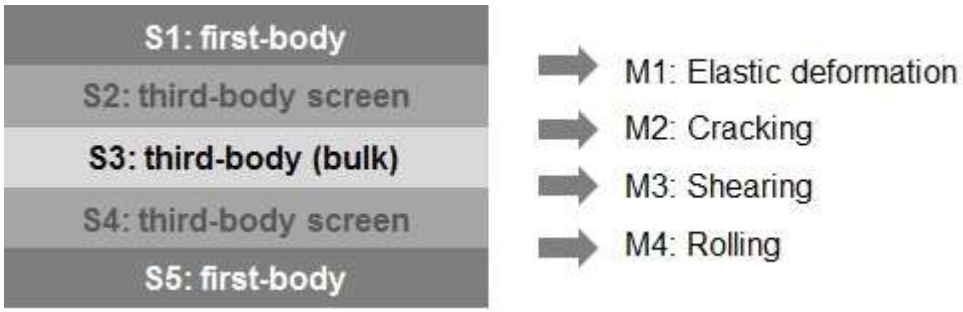
S1: first-body
S2: third-body screen
S3: third-body (bulk)
S4: third-body screen
S5: first-body
M1: Elastic deformation
M2: Cracking
M3: Shearing
M4: Rolling

Figure 2

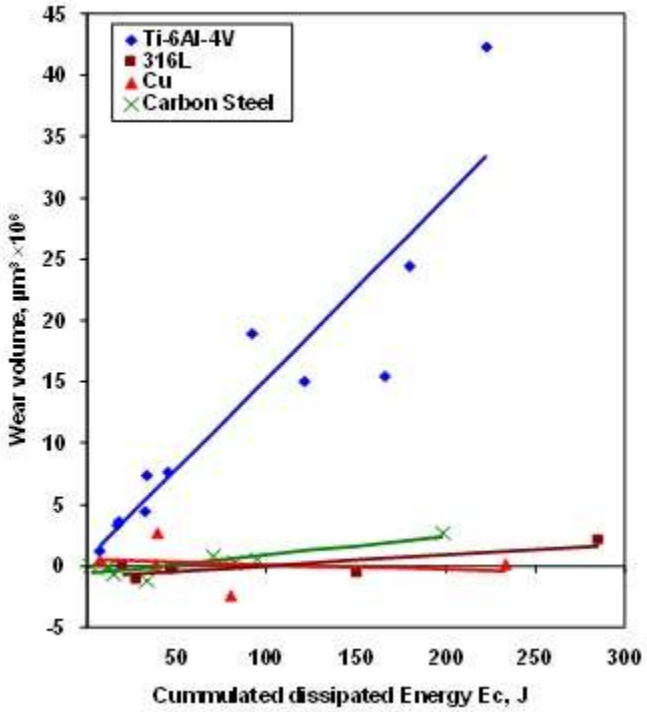
Ti-6Al-4V
316L
Cu
Carbon Steel
Wear volume, µm³ ×10⁶
Cummulated dissipated Energy Ec, J
45
40
35
30
25
20
15
10
5
0
-5
50
100
150
200
250
300

Figure 3

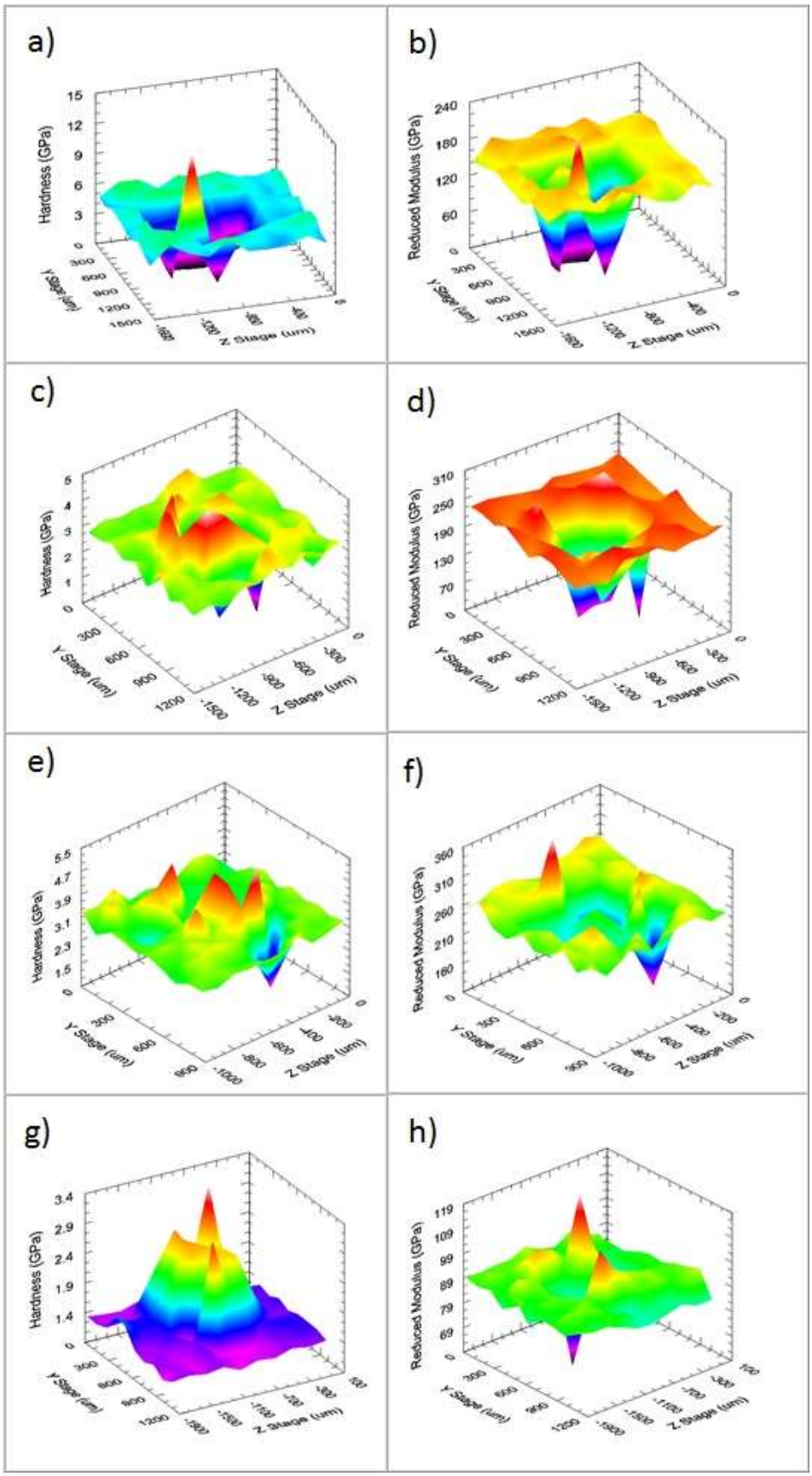
a)
Hardness (GPa)
Y Stage (um)
Z Stage (um)
b)
Reduced Modulus (GPa)
Y Stage (um)
Z Stage (um)
c)
Hardness (GPa)
Y Stage (um)
Z Stage (um)
d)
Reduced Modulus (GPa)
Y Stage (um)
Z Stage (um)
e)
Hardness (GPa)
Y Stage (um)
Z Stage (um)
f)
Reduced Modulus (GPa)
Y Stage (um)
Z Stage (um)
g)
Hardness (GPa)
Y Stage (um)
Z Stage (um)
h)
Reduced Modulus (GPa)
Y Stage (um)
Z Stage (um)

Figure 4

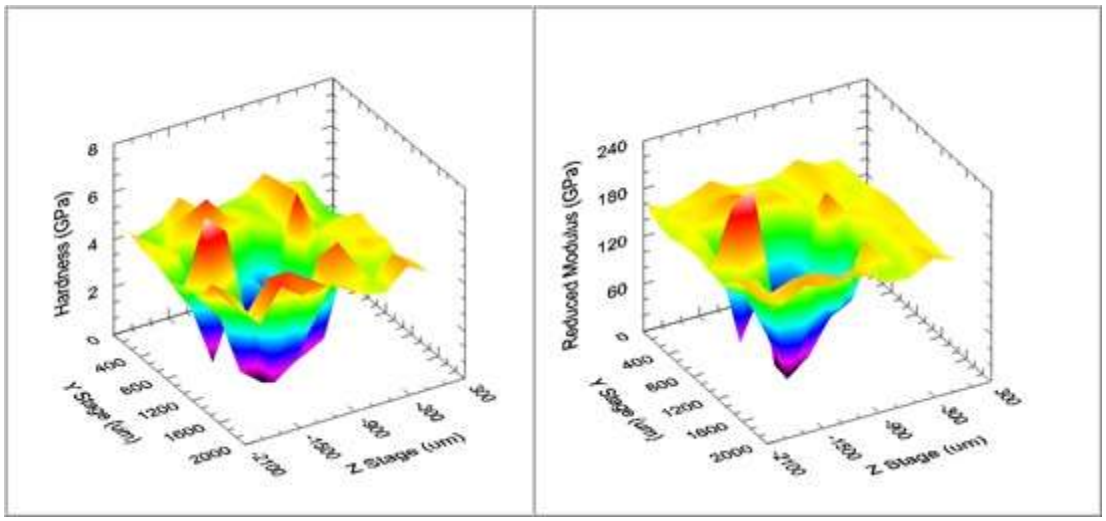
Hardness (GPa)
8
6
4
2
0
400
800
1200
1600
2000
Y Stage (um)
-2100
-1500
-900
-300
300
Z Stage (um)
Reduced Modulus (GPa)
240
180
120
60
0
400
800
1200
1650
2000
Y Stage (um)
-2100
-1500
-900
-300
300
Z Stage (um)

Figure 5

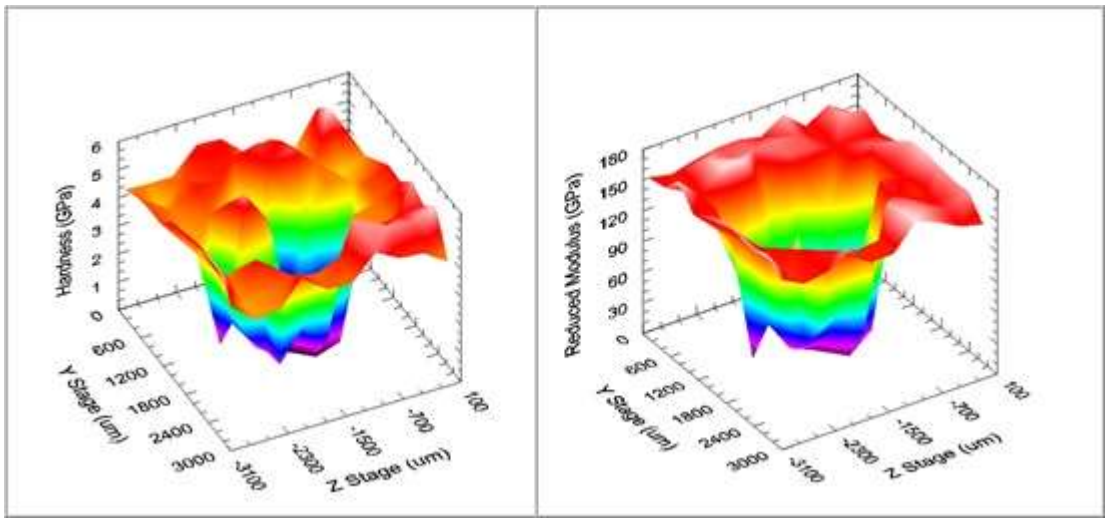
Hardness (GPa)
0
1
2
3
4
5
6
Y Stage (um)
600
1200
1800
2400
3000
Z Stage (um)
-3100
-2300
-1500
-700
100
Reduced Modulus (GPa)
0
30
60
90
120
150
180
Y Stage (um)
600
1200
1800
2400
3000
Z Stage (um)
-3100
-2300
-1500
-700
100

Figure 6

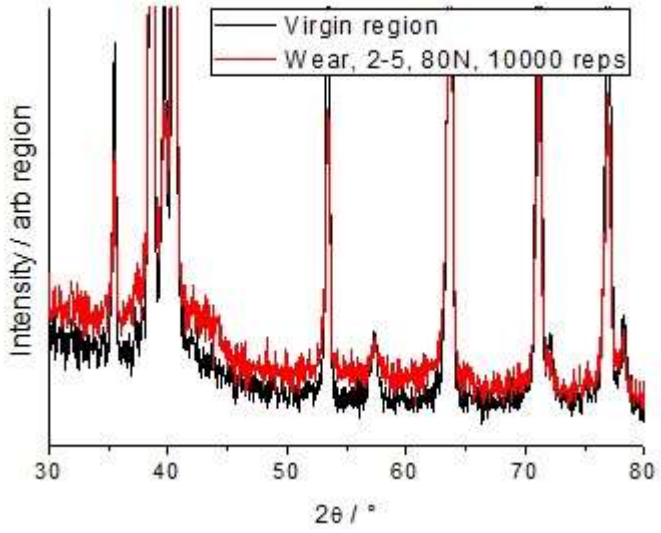
Virgin region
Wear, 2-5, 80N, 10000 reps
Intensity / arb region
30
40
50
60
70
80
2θ / °

Figure 7

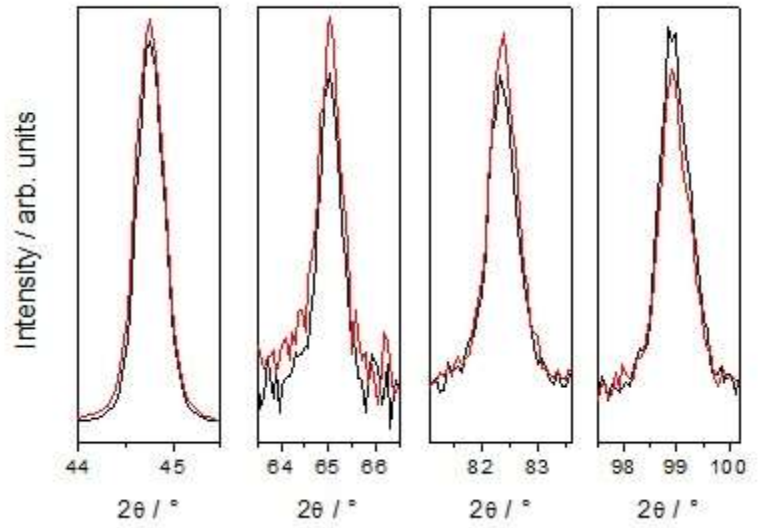

Figure 8

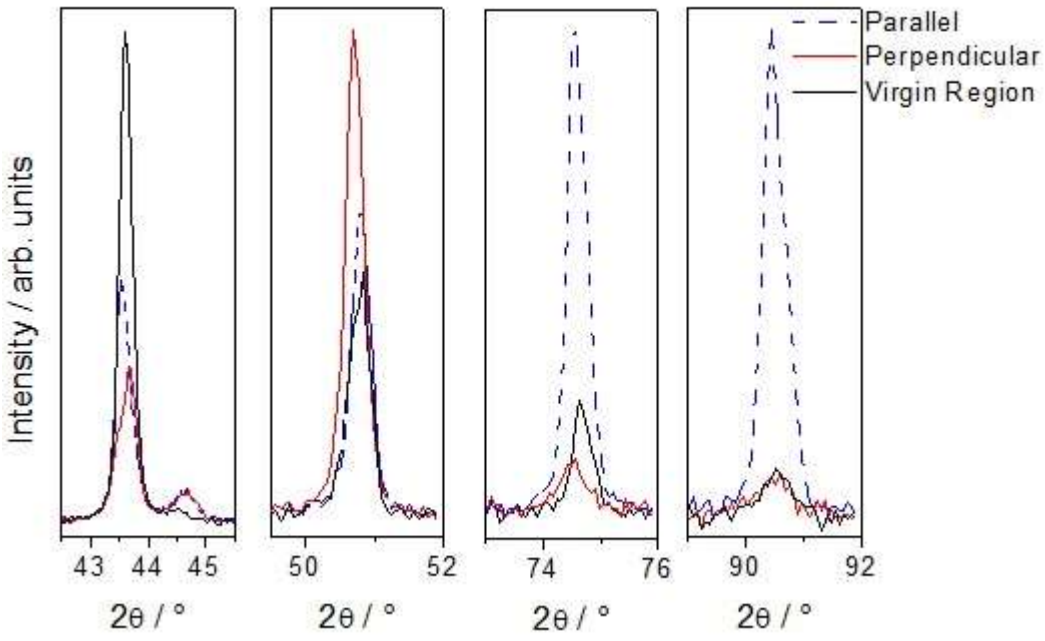
Parallel
Perpendicular
Virgin Region
Intensity / arb. units
43
44
45
2θ / °
50
52
2θ / °
74
76
2θ / °
90
92
2θ / °

Figure 9

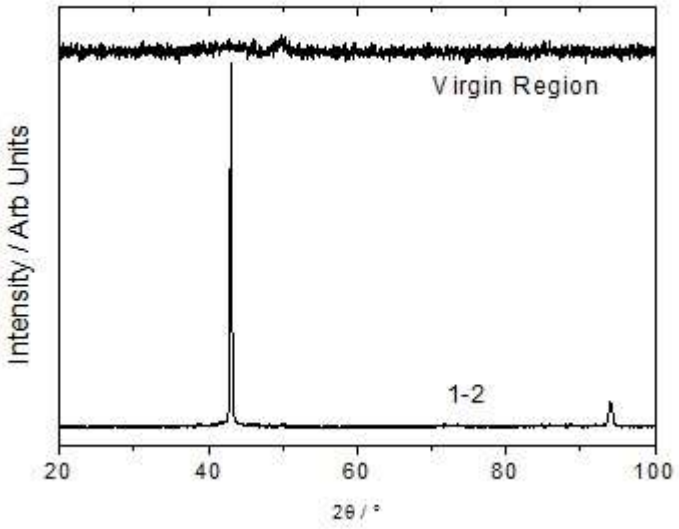

Figure 10

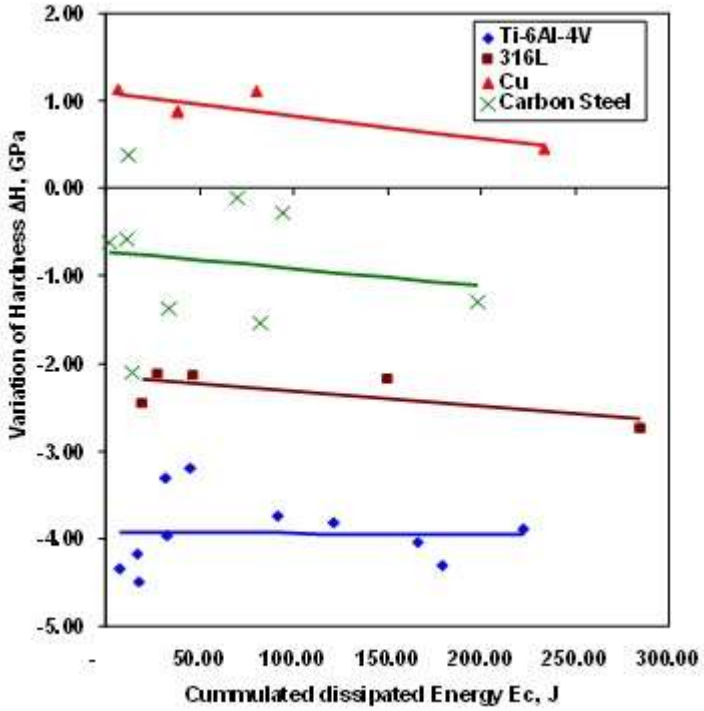
Ti-6Al-4V
316L
Cu
Carbon Steel
Variation of Hardness ΔH, GPa
2.00
1.00
0.00
-1.00
-2.00
-3.00
-4.00
-5.00
-
50.00
100.00
150.00
200.00
250.00
300.00
Cummulated dissipated Energy Ec, J

Figure 11

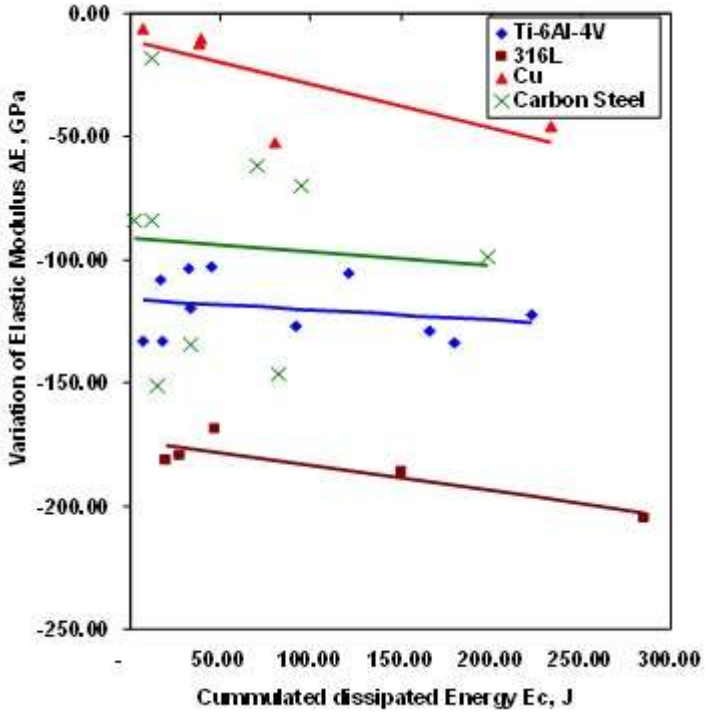
0.00
-50.00
-100.00
-150.00
-200.00
-250.00
Variation of Elastic Modulus ΔE, GPa
-
50.00
100.00
150.00
200.00
250.00
300.00
Cummulated dissipated Energy Ec, J
Ti-6Al-4V
316L
Cu
Carbon Steel